THE ASTROPHYSICAL JOURNAL, 165:265–284, 1971 April 15

EXTENDED MODEL ATMOSPHERES FOR THE CENTRAL STARS OF PLANETARY NEBULAE

JOSEPH P. CASSINELLI*
University of Washington, Seattle, Washington 98105
Received 1970 October 28; revised 1970 November 20

ABSTRACT

Procedures for the construction of spherical stellar model atmospheres are developed and applied to the calculation of three gray and three nongray model atmospheres for the central stars of planetary nebulae. The models are calculated under the classical assumptions of hydrostatic, radiative, and local thermodynamic equilibrium. Radiative transfer for spherical geometry and the $1/r^2$ dependence of gravity are taken into account. The transfer equation is solved by using the discrete-S_N method of Carlson and Lathrop and a difference form of the diffusion-approximation equation. The atmospheres are brought to radiative equilibrium by using modifications to spherical geometry of the flux-correction procedure of Unsöld for the gray case, and of the temperature-correction procedure of Lucy for the nongray case. Models which have luminosity constant with r to within 1.5 percent are calculated. All of the models have the same geometrical extension, and in each case the geometrical depth from $\langle\tau\rangle = 0.001$ to $\langle\tau\rangle = 1.0$ is approximately equal to the radius of curvature of the atmosphere at $\tau = 1.0$. The three nongray models have temperatures, at $\langle\tau\rangle = \frac{2}{3}$, of 3.7×10^{4}°, 4.9×10^{4}°, and 9.5×10^{4}° K. The emergent continuous flux of the models shows emission edges at the Balmer and Lyman limits and strong absorption edges in the far-ultraviolet. These features are explained as being due to the rapid increase of the temperature with optical depth and by geometrical enhancement of the Schuster mechanism. The flux distribution in the visual and infrared matches rather well the continuum of the Wolf-Rayet stars observed by Kuhi.

I. INTRODUCTION

Model atmospheres for the central stars of planetary nebulae have been calculated by Gebbie and Seaton (1963), Böhm and Deinzer (1965, 1966), Gebbie (1967), Böhm (1969), and Hummer and Mihalas (1970). In all cases the classical assumptions of hydrostatic, radiative, and local thermodynamic equilibrium were used, as well as the assumption of plane-parallel stratification. The latter assumption is valid if the mean free path of a photon is small compared with the radius of curvature of the atmospheric layers and if the acceleration of gravity is nearly constant over these layers. Böhm (1969) and Böhm and Cassinelli (1970) have summarized arguments that some central stars may have extended atmospheres owing to the effects of radiation pressure. These stars lie near the radiative-instability limit, defined by

$$|g| = |g_{\rm rad}| \approx \frac{\sigma^* T_{\rm eff}^4}{c}\sigma\,, \tag{1}$$

where g is the surface gravity of the star, $g_{\rm rad}$ is the radiative-pressure gradient, σ^* is the Stefan-Boltzmann constant, and σ is the Thomson-scattering coefficient. Böhm (1969) calculated plane-parallel models with surface gravities approaching the instability limit. He found hydrostatic atmospheres with a geometrical thickness down to $\langle\tau\rangle = 1.0$, larger than 1 stellar radius if the instability limit was approached to within $g_{\rm rad} \approx 0.9|g|$. In such an atmosphere the effects of curvature in the atmospheric layers become very important.

To gain some understanding of the effect of geometrical extension on the atmospheric

* Present address: The Joint Institute for Laboratory Astrophysics, University of Colorado, Boulder, Colorado 80302.

structure and on the energy distribution of the emergent flux, we have computed spherical model atmospheres, taking into account the radial variation of gravity and radiative transfer in spherical geometry. To isolate the effects of geometrical extension, we make the assumptions of hydrostatic, radiative, and local thermodynamic equilibrium. The usual procedures for calculating model atmospheres require considerable modification before they can be applied to the calculation of spherical model atmospheres.

The radiative transfer in spherical geometry is calculated by using discretization methods in which it is assumed that the atmosphere is composed of constant property shells. The discretization into shells is defined by a dimensionless variable ζ, which is used as the independent variable in the hydrostatic calculation.

Radiative equilibrium is enforced by using modifications for spherical geometry of the temperature correction procedures of Unsöld (1951) for the gray case, and of Lucy (1964) for the nongray case. The resulting models have a luminosity, $L(r)$ versus r which deviates from a constant value by less than 1 percent in the gray case and by less than 1.5 percent in the nongray case.

Mihalas (1967) has reviewed methods for computing plane-parallel model atmospheres. These models are specified by the chemical composition, the effective temperature T_{eff}, and the surface gravity g. A reasonable first approximation to the temperature stratification is provided by the analytic solution to the gray problem:

$$T^4 = \tfrac{3}{4}T_{\text{eff}}^4[\tau + q(\tau)]\,, \tag{2}$$

where $q(\tau)$ is the well-known Hopf function.

In an extended atmosphere, the "radius" of the star, say at $\tau_\nu = 1$, varies greatly with frequency; thus the terms "surface gravity" and "effective temperature" become ambiguous. Furthermore, there is no general solution for the temperature stratification, even for the gray case, because as Chapman (1964) has stressed, in a spherical atmosphere the radiation field and therefore the radiative-equilibrium temperature depends explicitly on the distribution of sources of opacity with depth. We have found it necessary to iterate by using a flux-correction procedure to get even the gray structure of the atmosphere. We have found no simple generalizations of the concepts of effective temperature and surface gravity for the spherical case. In place of these, we specify the atmospheres for computational purposes by the following quantities: (*a*) the mass M of the star; (*b*) the geometrical extension of the atmospheric layers, say $R_{\text{max}} = 4 \times R_{\text{min}}$; (*c*) the optical depth at the "top" of the atmosphere, $\langle\tau_{\text{min}}\rangle$; and (*d*) the optical depth at the "bottom" of the atmosphere, $\langle\tau_{\text{max}}\rangle$. The luminosity of the star is roughly determined by the necessity that the outward acceleration owing to radiation-pressure effects nearly compensates for the inward acceleration of gravity. For our models we find that the ratio of radiative to gravitational accelerations is given by

$$0.80 < \frac{\sigma L}{4\pi cGM} < 0.93\,. \tag{3}$$

The statement that $\langle\tau\rangle = \tau_{\text{min}}$ ($\approx .001$) at the top of the atmosphere leads to a boundary condition on the gas pressure. The requirement that $\langle\tau\rangle = \tau_{\text{max}}$ (≈ 10 or 15) at the lower boundary, $r = R_{\text{min}}$, is made to ensure that the atmosphere is indeed extended in the sense that the mean free path is not negligibly small compared with the radius of curvature in the atmosphere. This requirement is satisfied by making small changes in the ratio of radiative to gravitational accelerations. We shall find that we have some hold on the temperature range in the atmosphere because the spherical-distribution $B(\tau)$ is roughly bounded by the plane-parallel $B(\tau)$ evaluated by using the flux (ergs cm^{-2}) at the inner and at the outer radii of the atmospheric layers.

In following sections we discuss in detail the equations in spherical geometry of

hydrostatic equilibrium and of radiative transfer. Unlike the plane-parallel case, the equations cannot in general be expressed in terms of optical depth as the independent variable because of the explicit appearance of the position variable r in the equations.

II. THE EQUATION OF HYDROSTATIC EQUILIBRIUM

The hydrostatic equation is

$$\frac{dP}{dr} = -\frac{GM\rho}{r^2} + \frac{k_F \rho L}{4\pi r^2 c}, \tag{4}$$

where G is the gravitational constant, P is the gas pressure, ρ is the density, k_F is the flux mean opacity, and c is the speed of light. The last term is the radiative-pressure gradient. Factoring out the gravitational term, we obtain

$$\frac{dP}{dr} = -\frac{GM\rho}{r^2}\left(1 - \frac{k_F}{\sigma_0}\gamma^*\right), \tag{5}$$

where

$$\gamma^* = \frac{\sigma_0 L}{4\pi c G M} \tag{6}$$

is the ratio of the radiative-pressure gradient to the acceleration of gravity for the case of pure electron scattering in a completely ionized gas, in which $\sigma = \sigma_0 (= 0.306)$.

Using the equation of state,

$$P = \rho k T / \langle \mu \rangle m_{\rm H}, \tag{7}$$

and introducing

$$\zeta \equiv \frac{GM m_{\rm H}}{k T_1 r} = \frac{\text{constant}}{r} = \frac{A_\zeta}{r}, \tag{8}$$

we modify equation (5) to read

$$\frac{d \ln P}{d\zeta} = \frac{\langle \mu(\zeta) \rangle}{T(\zeta)/T_1}\left(1 - \frac{k_F}{\sigma_0}\gamma^*\right). \tag{9}$$

In these equations k is Boltzmann's constant, $m_{\rm H}$ is the mass of a hydrogen atom, $\langle \mu \rangle$ is the mean molecular weight, and T_1 is some reference temperature (10^5 ° K). This equation formally integrates to

$$P = P_0 \exp\left[+\int_{\zeta_0}^{\zeta} \frac{\langle \mu(\zeta) \rangle}{T(\zeta)/T_1}\left(1 - \frac{k_F}{\sigma_0}\gamma^*\right) d\zeta\right], \tag{10}$$

where P_0 is the boundary pressure at $\zeta = \zeta_0$. In the isothermal case in which $\langle \mu \rangle =$ constant and $k_F = \sigma_0$, the hydrostatic solution takes the simple form

$$P = P_0 \exp\,(+\xi - \xi_0), \tag{11}$$

where

$$\xi = \frac{\langle \mu \rangle}{T/T_1}(1 - \gamma^*)\zeta = \frac{A_\xi}{r}, \tag{12}$$

so

$$d\xi = -\frac{dr}{H}, \tag{13}$$

where H is the scale height $kT/\langle \mu \rangle m_{\rm H} g_{\rm eff}$. Equation (13) states that in regions where k_F and $\langle \mu \rangle$ are constant, equal steps in ξ (or ζ) correspond to radial steps proportional to the local scale height, and (from eq. [11]) to equal steps in the logarithm of pressure.

This feature is desirable for the calculations of radiative transfer. In the hot atmospheres considered here, the mean opacity does not deviate far from the electron-scattering value and the mean molecular weight is nearly constant everywhere.

In the plane-parallel case a boundary condition on the pressure may be derived by assuming that the atmosphere above the first optical-depth point is isothermal with only electron scattering contributing to the opacity. For this case the density distribution is $\rho = \rho_0 e^{-h/H}$ and we find that

$$\tau_{\min} = -\int_0^\infty \rho\sigma dh = \rho_0 \sigma H \tag{14}$$

and ρ_0 is related to P_0 by equation (7). In the spherical case this procedure for determining the boundary pressure encounters difficulties because $\rho = \rho_0 \exp(\xi - \xi_0)$ remains finite at infinity and the optical depth integral

$$\tau_{\min} = A_\xi \int_0^{\xi_0} \rho_0 \exp(\xi - \xi_0)\sigma \frac{d\xi}{\xi^2} \tag{15}$$

diverges. The solution lies in the realization that in an actual atmosphere the hydrostatic distribution does not hold at large distances from the star. Spherical hydrostatic atmospheres are considered also in the theory of planetary exospheres. Chamberlain (1963) considers the number-density distribution far out in a planetary atmosphere where collisions between the atmospheric constituents are rare. He finds that as radial distance from the planet increases, the density falls increasingly below what is given by the hydrostatic distribution because the angular distribution of particle velocity vectors becomes increasingly concentrated in the direction of the outward radius vector. He shows that for $\xi_0 \gg 1$ the lower limit on the optical-depth integral, equation (15), should be changed from $\xi = 0$ to $\xi = 1$ to account for the deviation from the hydrostatic law. Adopting Chamberlain's cutoff, we find

$$\tau_{\min} = \sigma \rho_0 H_0 K(\xi_0) , \tag{16}$$

where

$$K(\xi_0) = \int_1^{\xi_0} \frac{\xi_0^2}{\xi^2} \exp[-(\xi_0 - \xi)] d\xi \approx 1 + \frac{2}{\xi_0} \text{ for } \xi_0 \gg 1 , \tag{17}$$

so

$$\tau_{\min} = \sigma \rho_0 H_0 \left(1 + \frac{2}{\xi_0}\right), \tag{18}$$

an expression which closely resembles the plane-parallel result, equation (14). In our model calculations we take $\tau_{\min} = 0.001$ as the first optical-depth point.

III. RADIATIVE TRANSFER IN SPHERICAL ATMOSPHERES

The transfer equation in spherical geometry may be written

$$\left[\mu \frac{\partial}{\partial r} + \frac{(1 - \mu^2)}{r} \frac{\partial}{\partial \mu}\right] I_\nu(r, \mu) = -k_\nu \rho (I_\nu - S_\nu) , \tag{19}$$

where μ is the cosine of the angle θ between the beam of radiation and the outward radial direction; k_ν is the total extinction coefficient at frequency ν per gram, and is the sum of κ_ν, the true absorption coefficient, and σ, the scattering coefficient. The source function S_ν is

$$S_\nu = \frac{\kappa_\nu B_\nu + \sigma J_\nu}{\kappa_\nu + \sigma} \tag{20}$$

for the nongray case and

$$S = B$$

for the gray case, where B_ν is the Planck function, J_ν is the mean intensity (averaged over all directions) and $B = \sigma^* T^4/\pi$. We assume that the scattering is isotropic, coherent, and independent of frequency.

The basic problem with radiative transfer in spherical geometry is that the angular coordinate system changes with geometrical position, i.e., $\mu = \mu(r)$. Thus as a photon travels through the atmosphere, its coordinate μ is constantly changing, even though the photon does not physically change direction. In the transfer equation the $\partial/\partial\mu$ term accounts for the directional transfer. We have used two numerical schemes to solve the transfer equation, (*a*) the discrete-S_N method, and (*b*) a standard-difference form of the transfer equation under the Eddington approximation (a diffusion-approximation equation). In the discrete-S_N method, "curvature coefficients" are introduced into a discrete form of the transfer equation to account for the direction transfers. In the diffusion-approximation calculation only mean intensities, integrated over all angles, are involved and so in a sense the direction changes are integrated out of the equations.

a) The Discrete-S_N Method

This method is a numerical version of the discrete-ordinates method developed by B. G. Carlson and his collaborators for calculations of neutron transport in reactors. It differs from the discrete-ordinates method of Chandrasekhar (1950) in that both the angular variable μ *and* the space variable r are discretized. Detailed reviews of the method are given by Carlson (1963) and Carlson and Lathrop (1968), where the discretized form of the transfer equation is derived by considering conservation relations for a finite cell in phase space (r_i, μ_m) and the resultant expression is shown to reduce to the spherical transfer equation in the limit of small spatial and angular intervals. The discrete transfer equation is presented in the Appendix. It is solved in a recursive manner, one direction at a time, by starting at the outer boundary, where $I(r, \mu_m^-)$ is known from the boundary condition, and then stepping in toward the inner boundary. The solution is completed by a similar recursive march, for each of the outward directions μ_m^+, starting with boundary conditions specified at the inner boundary. The numerical method that carries out the solution for $I(r_i, \mu_m)$ is essentially the same as that of Lathrop (1965), but as reformulated in the notation of radiative transfer by Stoddard (1969).

In the nongray problem, large variations of κ_ν occur in going from the long-wavelength side of an absorption edge to the short-wavelength side. (The κ_ν may increase by as much as a factor of 10^3.) Thus the spherical shells may have a large range in monochromatic optical depth, $\Delta\tau_\nu$. The discrete-S_N method is not accurate for step sizes of large optical depth. For this reason we do not use the full discrete-ordinate formalism at all depths and at all frequencies. Instead, we use diffusion-approximation results at large optical depth where the radiation field is nearly isotropic, and fit the discrete-ordinate calculation onto this so that the mean intensity J_ν and the flux H_ν are continuous at the fitting point. At frequencies where $\kappa_\nu \gg \sigma_{es}$ even this procedure is not practical, and the diffusion-approximation results are used all the way to the surface.

b) The Diffusion-Approximation Equations

Operating on the transfer equation with the moment operators $\mathfrak{M}_0$ and $\mathfrak{M}_1$, where

$$\mathfrak{M}_n f = \tfrac{1}{2} \int_{-1}^{+1} f \mu^n d\mu \,, \tag{21}$$

we obtain, after performing an integration by parts on the $\partial/\partial\mu$ term, the moment equations

$$\frac{1}{r^2}\frac{d}{dr}(r^2 H_\nu) = -k_\nu \rho (J_\nu - S_\nu) \tag{22}$$

$$\frac{dK_\nu}{dr} + \frac{1}{r}(3K_\nu - J_\nu) = -k_\nu \rho H_\nu , \tag{23}$$

where

$$J_\nu(r) = \mathfrak{M}_0[I_\nu(r, \mu)] ; \quad H_\nu = \mathfrak{M}_1[I_\nu(r, \mu)] ; \quad K_\nu = \mathfrak{M}_2[I_\nu(r, \mu)] . \tag{24}$$

Further operations on the transfer equation with ever higher moment operators $\mathfrak{M}_n$ will yield equations containing ever higher moments. The system is brought to closure by using a "terminating condition." The moment K_ν may be eliminated from equations (22) and (23) by representing the intensity as a first-order polynomial,

$$I_\nu(r, \mu) = a_0(r) + a_1(r)\mu . \tag{25}$$

Applying $\mathfrak{M}_n$ to this expression for $n = 0, 1, 2$, we find

$$K_\nu = \tfrac{1}{3} J_\nu , \tag{26}$$

the well-known Eddington approximation. Using this in equation (23), we obtain

$$H_\nu = -\frac{1}{3k_\nu \rho}\frac{dJ_\nu}{dr} ; \tag{27}$$

then, by combining equation (27) with equations (22) and (20) and using $k_\nu = \kappa_\nu + \sigma$, we obtain

$$\frac{1}{r^2}\frac{d}{dr}\left(\frac{r^2}{3(\kappa_\nu + \sigma)\rho}\frac{dJ_\nu}{dr}\right) = -\kappa_\nu \rho (J_\nu - B_\nu) , \tag{28}$$

which is the diffusion approximation equation or the "transfer equation under the Eddington approximation."

The equation is expressed in difference form and written as a tridiagonal matrix

$$a_k J_{k+1} - b_k J_k + c_k J_{k+1} = -d_k \tag{29}$$

which is solved by a Gaussian elimination scheme (Wachspress 1966).

c) Boundary Conditions

The general form of the boundary condition at $R_{\min}$ and $R_{\max}$ for the diffusion equation is $\alpha J_\nu + \beta(dJ_\nu/dr) = \gamma$. At the top of the atmosphere we assume there is no incoming radiation,

$$I(R_{\max}, \mu^-) = 0 , \tag{30}$$

which may be expressed in terms of the moments J_ν and H_ν as

$$H_\nu(0) = \frac{1}{3^{1/2}} J_\nu(0) = \frac{-1}{3(\kappa_\nu + \sigma)\rho}\frac{dJ_\nu}{dr}\bigg|_0 \tag{31}$$

(Krook 1955). At the inner boundary, we use a condition which should be valid asymptotically at large depth. We assume, as is done in the derivation of the Rosseland mean, that $dJ_\nu/d\tau_\nu = dB_\nu/d\tau_\nu$ so that

$$H_\nu = \frac{-1}{3(\kappa_\nu + \sigma)\rho}\frac{dB_\nu}{dr} . \tag{32}$$

If $\langle \kappa_\nu + \sigma \rangle$ is the Rosseland mean, then

$$H = \frac{-1}{3\langle \kappa_\nu + \sigma \rangle \rho}\frac{dB}{dT}\frac{dT}{dr} , \tag{33}$$

so that

$$\frac{H_\nu}{H} = \frac{\langle \kappa_\nu + \sigma \rangle}{(\kappa_\nu + \sigma)} \frac{dB_\nu/dT}{dB/dT}, \tag{34}$$

where H is related to the total luminosity by

$$4\pi H = \frac{L}{4\pi R_{\min}{}^2}. \tag{35}$$

For the discrete-ordinate calculation we may use equation (30) at $r = R_{\max}$. At large optical depths we assume that the results of the diffusion calculation for J_ν and H_ν are accurate and we assume, following equation (25), that the linear expression $I = a + b\mu^+$ is valid for the outward-directed radiation alone. Values for a and b may be calculated from

$$J_\nu(r^*) - J_\nu^- = a\Sigma^+ w_m + b\Sigma^+ w_m\mu_m\,, \quad H_\nu(r^*) - H_\nu^- = a\Sigma^+ w_m\mu_m + b\Sigma^+ w_m\mu_m{}^2\,, \tag{36}$$

where r^* is the fitting point and corresponds to an optical depth $\tau_\nu \approx 10$. $J_\nu(r^*)$ and $H_\nu(r^*)$ are the diffusion-approximation results at r^*; and

$$J_\nu^- = \Sigma^- I_\nu(r^*, \mu_m^-) w_m\,, \quad H_\nu^- = \Sigma^- I_\nu(r^*, \mu_m^-) w_m\mu_m^- \tag{37}$$

are moment sums over the inward-directed intensities, which are known from the inward-directed discrete-S_N recursive marches.

Thus the diffusion calculations are used to extrapolate the lower boundary condition from $R_{\min}$ to r^*.

d) Source-Function Iteration

When scattering is involved, the solution to the transfer equation by the discrete-S_N method requires iteration because the source function (20) involves J_ν, which is an integral over $I_\nu(r, \mu)$, but I_ν is not known until the solution is in progress. Fortunately, the computation time required to find $J_\nu(r)$ for a given source function is short (<0.3 sec on a CDC 6400), but a convergence-acceleration scheme is necessary nonetheless. A number of such schemes exist. Here we use a procedure proposed by Gelbard and Hageman (1969). If $R^n(r)$ is the change in $J_\nu(r)$ in going from the nth to the $(n+1)$th iteration, the Gelbard and Hageman procedure prescribes that the source function for the next iteration will be computed with

$$J^{n+1} = J^n + R^n + \Lambda_d\{\sigma R^n\}\,, \tag{38}$$

where the last term represents a diffusion-approximation calculation which uses σR^n as a source term. Even if we use equation (38), the convergence of the iterations is monotonic: successive calculations are everywhere closer to the true solution; but if $J^n < J^{\text{true}}$ everywhere, then $J^{n+1} < J^{\text{true}}$ everywhere. It is desirable to use an overestimate of the correction so that J^{n+1} lies on the opposite side of J^{true} than did J^n, for then the true solution is bracketed. To achieve this overshoot we use the fact that in successive iterations the monochromatic flux $H_\nu(r)$ also converges monotonically toward a final value. Thus the convergence-acceleration procedure is as follows:

$$J^{n+1} = J^n + R^n + \Lambda_d\{\sigma R^n\} + \Lambda_h\{\Delta H\}\,, \tag{39}$$

where

$$\Lambda_h\{\Delta H\} = 3\int_r^{R_{\max}} k\rho(\Delta H_\nu)^n dr \tag{40}$$

and

$$(\Delta H_\nu)^n = H_\nu{}^{n+1} - H_\nu{}^n\,. \tag{41}$$

Equations (38) and (39) are used on alternate iterations, starting with the third, until overshoot occurs. Then only equation (38) is used until

$$\frac{|J^{n+1} - J^n|}{0.5|J^{n+1} + J^n|} < 0.5 \times 10^{-4} \tag{42}$$

at all optical depths. The scheme was tested on a gray-atmosphere calculation for which a good run of $J(r)$ was known from the Unsöld flux-correction procedure which will be discussed in § IV. The results agree to within 1 percent at all depths.

e) Comparison with Other Work

Most of the astronomical literature on the solution of the spherical radiative-transfer equation has been concerned with the gray case in which $k\rho$ is inversely related to radius ($k\rho = 1/r^n$). In such a case the transfer equation may again be expressed with optical depth as the independent variable (see, e.g., Chandrasekhar 1950; Kosirev 1934). Chapman (1964, 1966) has obtained a near-radiative-equilibrium solution for the case $n = 3$. For this value of n he finds that the solution for J is given approximately by

$$J(\tau) = \tfrac{3}{4}r^2H(4\tau^2 + 3.077\tau) . \tag{43}$$

Our results and Chapman's agree to within 5 percent. The radiative transfer for this comparison was calculated by using the discrete-S_N method, and the "boundaries" of the atmosphere were placed at $\tau = 20$ and at $\tau = 0.05$, with $\tau(r) = 0.5r^{-2}$. The Eddington-approximation result was used as the initial guess to the source-function stratification, and the Unsöld flux-correction procedure described in § IV was used to achieve radiative equilibrium. Flux constancy to <0.1 percent was achieved in six iterations. The calculations were made by using a three-point double-Gauss angular quadrature (for a total of six directions, i.e., an S_6 representation) and using 60, 90, and 120 radial steps. (The results of these cases were nearly identical.)

Recently Schmid-Burgk (1970) has developed an accurate numerical scheme for solving the $1/r^n$ problem. The results of the discretization scheme used here agree to within a few percent with those of Schmid-Burgk.

IV. RADIATIVE EQUILIBRIUM: THE TEMPERATURE CORRECTION PROCEDURES

For a spherical atmosphere in radiative equilibrium, the total radiative luminosity flowing through the atmosphere is independent of depth, or

$$r^2\int_0^\infty H_\nu d\nu = \frac{L}{(4\pi)^2} \equiv H^0 = \text{constant} . \tag{44}$$

This expression follows from equation (22) if one uses equation (20) and the usual form of the radiative-equilibrium condition,

$$\int_0^\infty \kappa_\nu B_\nu d\nu = \int_0^\infty \kappa_\nu J_\nu d\nu .$$

In addition to the $1/r^2$ dependence of flux, Chapman (1966) notes that, very far out in the atmosphere, the radiation field is concentrated in the radial direction; and thus

$$J \approx H \approx K . \tag{45}$$

The model atmospheres calculated here are moderately compact, and a satisfactory flux-correction procedure may be derived by using the moment equations under the

Eddington approximation $K = \frac{1}{3}J$. But it is of interest to note that a very similar correction procedure could be derived with the closure condition $K = J$.

After the radiative-transfer calculation is completed, the departure from constancy of r^2H may be calculated:

$$\Delta H^0(r) = r^2H(r) - R_{\min}{}^2H(R_{\min}) . \tag{46}$$

The temperature distribution is then corrected. For the gray case, the correction to the source function $B(r)$ is

$$\Delta B(r) = -\left[\frac{\Delta H^0(R_{\max})}{R_{\max}{}^2} + 3\int_r^{R_{\max}} k\rho \frac{\Delta H^0(r)}{r^2}\, dr\right] + J(r) - B(r) . \tag{47}$$

The derivation of this equation is a straightforward modification of Unsöld's (1951) flux-correction procedure, except that the spherical-moment equations (22) and (23) are used instead of the planar-moment equations. Also, instead of using the Eddington expression $H = \frac{1}{2}J$ we here use $H = J$ at the surface, following equation (45).

For the nongray correction, we use a similar modification of the Lucy (1964) procedure:

$$\Delta B(r) = -\frac{\kappa_J}{\kappa_p}\left[\frac{\Delta H^0(R_{\max})}{R_{\max}{}^2} + 3\int_r^{R_{\max}} k_F\rho \frac{\Delta H^0}{r^2}\, dr\right] + \left[\frac{\kappa_J}{\kappa_p} J(r) - B(r)\right]$$

$$= \Delta B_1 + \Delta B_2 , \tag{48}$$

where ΔB_2 is the second bracketed term and κ_J, κ_p, and k_F are mean absorption coefficients:

$$\kappa_p = \frac{1}{J}\int_0^\infty \kappa_\nu J_\nu d\nu ; \quad \kappa_p = \frac{1}{B}\int_0^\infty \kappa_\nu B_\nu d\nu ; \quad k_F = \frac{1}{H}\int_0^\infty (\kappa_\nu + \sigma) H_\nu d\nu . \tag{49}$$

Equation (48) is derived under the assumption that the mean opacities κ_J, κ_p, and k_F do not change from one iteration to the next as significantly as J, B, and H. We found it best to use just a fraction (≈ 0.5) of the ΔB_2 part of the correction if $\Delta B_2/B > 0.1$, following the suggestion of Lucy (1964).

After six iterations, Unsöld's method achieved a flux constancy good to 1 percent, while Lucy's method achieved a flux constancy of 1.5 percent in nine iterations or less.

V. COMPUTATIONAL PROCEDURES

The calculation of extended model atmospheres differs from the planar case primarily because the models are specified not by $T_{\rm eff}$ and g but rather by the parameters given in § I. The hydrostatic-structure calculation proceeds as follows: For given values of $R_{\min}$ and $R_{\max}$, extreme values of ζ are calculated via equation (8). N equal steps in ζ define the discretization into spherical shells (r_i). The equation of hydrostatic equilibrium may be integrated if $T(r)$, the boundary P_0, and γ^* are specified. We use the Runge-Kutta method for the first four depth steps of the numerical integration and Hamming's (1962) method for the remaining steps. We approximate the radiative acceleration by using the Rosseland mean opacity instead of the flux mean k_F.

After the calculation of the hydrostatic structure, the mean and monochromatic optical depths are calculated, e.g., from

$$\langle\tau(\zeta)\rangle = A_\zeta \int_{\zeta_0}^{\zeta} \langle k\rangle\rho \frac{d\zeta}{\zeta^2} ; \tag{50}$$

and we could proceed to carry out the radiative-transfer calculations and the temperature corrections. Before this is done, a test is made on the total mean optical depth τ_{total} for the following reasons: There are two characteristic lengths in the spherical radiative-transfer problem, the radius of curvature of the atmospheric layers and the photon mean free path. This is in contrast to the planar case in which the geometrical coordinate plays no role in the transfer problem. So in our problem both the geometrical and optical properties must be specified in some way. We choose to specify the total geometrical thickness and the total mean optical depth of the atmospheric layers, τ_{max}. It is possible to satisfy the requirement that $\tau_{\text{total}} = \tau_{\text{max}}$ at the base of the atmosphere by adjusting the parameter γ^*, the ratio of radiative to gravitational acceleration in the atmosphere. If a single value of γ^* is used through a sequence of model iterations, the τ_{total} tends to drift far from its initial value, and thus the radiative properties of the atmosphere change grossly. The requirement that $\tau_{\text{total}} = \tau_{\text{max}}$ is enforced by using three different values of γ^* to calculate the hydrostatic structure, and τ_{total} is evaluated each time to form a set of (γ^*, τ_{total}). A Legendre interpolation is performed to find a γ^* that yields $\tau_{\text{total}} = \tau_{\text{max}}$, and the hydrostatic calculation is repeated once more before carrying out the radiative-transfer calculations, as discussed previously.

VI. RESULTS

Three sets of models have been calculated: three gray models and three nongray models. The temperature stratifications computed for the gray models were used as a first approximation in the nongray calculation. Parameters specifying the models are presented in Table 1. The chemical composition of the atmospheres was taken to be that used by Böhm and Deinzer (1965) (see Table 2 of that paper). The absorption coefficients were calculated by a subroutine of Böhm and Deinzer (1965) as modified by Böhm (1969). These calculations include the following contributions: bound-free transitions from the ground state of H, He, C III, C IV, N III, N IV, N V, O III, O IV, O V, O VI, Ne III, Ne IV, Ne V; bound-free transitions from low-lying levels of H, He I, and He II; free-free transitions of H, He I, and He II; and Thomson electron scattering. The frequencies used in the three sets of models are given in Table 2, with ionization-edge groupings as indicated.

In Tables 3–8 we present the hydrostatic run of temperature, pressure, density, and Rosseland mean opacity versus Rosseland mean optical depth for the models calculated. We have found no density inversions in any of these hydrostatic models. Such inversions would lead to an instability as discussed by Wentzel (1970).

TABLE 1

SUMMARY OF MODEL PARAMETERS

Parameter	Gray Model 1	Nongray Model 1	Gray Model 2	Nongray Model 2	Gray Model 3	Nongray Model 3
$M/M_\odot$	0.6	0.6	0.6	0.6	1.0	1.0
$R_{\text{min}}(10^{11}$ cm)	0.90	0.90	0.45	0.45	0.25	0.25
$R_{\text{max}}(10^{11}$ cm)	3.879	3.879	1.939	1.939	1.078	1.078
τ_{max}	10	10	10	10	15	15
τ_{min}	0.001	0.001	0.001	0.001	0.001	0.001
γ^*	0.8187	0.8045	0.8637	0.8584	0.9247	0.9290
$L/L_\odot \times 10^{-4}$	2.067	2.032	2.181	2.168	3.872	3.889
$T(2/3)$(°K)	34712	37496	53558	48864	82180	94681
No. of frequencies	24	24	24	24	33	33
No. of shells	60	60	60	60	90	90

TABLE 2

FREQUENCIES USED FOR THE SIX MODELS COMPUTED

ν(sec^{-1})	Ionization Edge
Gray Model 1 and Nongray Model 1	
0.3654×10^{15}	H I, $n=3$
0.5937×10^{15}	...
0.8220×10^{15}	H I, $n=2$
0.8221×10^{15}	
0.9871×10^{15}	...
1.1520×10^{15}	He I 2^3S
1.1530×10^{15}	
2.2205×10^{15}	...
3.2880×10^{15}	H I, $n=1$, and He II, $n=2$
3.2890×10^{15}	
4.6160×10^{15}	...
5.9440×10^{15}	He I, 1^1S
5.9450×10^{15}	
8.7025×10^{15}	...
1.1460×10^{16}	N III, C III
1.1470×10^{16}	
1.2310×10^{16}	...
1.3152×10^{16}	He II, $n=1$
1.3153×10^{16}	
1.5933×10^{16}	...
1.8714×10^{16}	O IV, N IV
1.8729×10^{16}	
2.9364×10^{16}	...
4.0000×10^{16}	...
Gray Model 2 and Nongray Model 2	
0.3654×10^{15}	H I, $n=3$
0.5937×10^{15}	...
0.8220×10^{15}	H I, $n=2$
0.8221×10^{15}	
1.1415×10^{15}	...
1.4610×10^{15}	He II, $n=3$
1.4620×10^{15}	
2.3745×10^{15}	...
3.2880×10^{15}	H I, $n=1$, and He II, $n=2$
3.2890×10^{15}	
4.6165×10^{15}	...
5.9440×10^{15}	He I, 1^1S
5.9450×10^{15}	
8.6530×10^{15}	...
1.1460×10^{16}	N III, C III
1.1470×10^{16}	
1.2310×10^{16}	...
1.3152×10^{16}	He II, $n=1$
1.3153×10^{16}	
1.5941×10^{16}	...
1.8714×10^{16}	O IV, N IV
1.8729×10^{16}	
2.9393×10^{16}	...
4.0000×10^{16}	...
Gray Model 3 and Nongray Model 3	
0.3654×10^{15}	H I, $n=3$
0.5937×10^{15}	...
0.8220×10^{15}	H I, $n=2$
0.8221×10^{15}	
1.1415×10^{15}	...
1.4610×10^{15}	He II, $n=3$
1.4620×10^{15}	
2.3745×10^{15}	...
3.2880×10^{15}	H I, $n=1$, and He II, $n=2$
3.2890×10^{15}	
4.6165×10^{15}	...
5.9440×10^{15}	He I, 1^1S
5.9450×10^{15}	
8.7025×10^{15}	...
1.1460×10^{16}	N III, C III
1.1470×10^{16}	
1.2311×10^{16}	...
1.3152×10^{16}	He II, $n=1$
1.3153×10^{16}	
1.5934×10^{16}	...
1.8714×10^{16}	O IV, N IV
1.8729×10^{16}	
2.1118×10^{16}	...
2.3507×10^{16}	Ne IV, N V
2.3665×10^{16}	
2.5617×10^{16}	...
2.7534×10^{16}	O V
2.7536×10^{16}	
2.9058×10^{16}	...
3.0581×10^{16}	Ne V
3.0583×10^{16}	
3.5292×10^{16}	...
4.0000×10^{16}	...

TABLE 3

GRAY MODEL 1: $T(2/3) = 34712$

τ_R	R (cm)	T (° K)	P (dyn cm^{-2})	ρ (g cm^{-3})	$\langle\kappa_R\rangle$ (cm^2 g^{-1})
.....	3.879(+11)	2.189(+4)	2.777(−1)	1.102(−13)	0.2707
1.269(−3).....	3.676	2.262	9.392	3.609	0.2739
4.489.....	3.493	2.338	2.892(+0)	1.075(−12)	0.2804
1.307(−2).....	3.328	2.423	7.790	2.794	0.2910
3.222.....	3.178	2.520	1.771(+1)	6.104	0.3048
1.251(−1).....	2.914	2.754	5.275	1.651(−11)	0.3348
2.001.....	2.798	2.881	7.108	2.106	0.3489
4.554.....	2.499	3.219	9.725	2.487	0.3657
6.870.....	2.259	3.498	1.243(+2)	2.891	0.3601
9.986.....	2.002	3.855	1.919	4.040	0.3558
2.014(+0).....	1.558	4.830	6.228	1.046(−10)	0.3513
3.071.....	1.349	5.626	1.361(+3)	1.961	0.3498
4.063.....	1.231	6.251	2.241	2.907	0.3504
5.006.....	1.150	6.773	3.169	3.793	0.3519
6.065.....	1.079	7.299	4.249	4.721	0.3541
7.212.....	1.017	7.817	5.433	5.635	0.3559
8.419.....	9.615(+10)	8.320	6.717	6.547	0.3570
9.985.....	9.000	8.972	8.552	7.729	0.3562

NOTE.—Numbers in parentheses indicate powers of 10.

TABLE 4

NONGRAY MODEL 1: $T(2/3) = 37496$

τ_R	R (cm)	T (° K)	P (dyn cm^{-2})	ρ (g cm^{-3})	$\langle\kappa_R\rangle$ (cm^2 g^{-1})
.....	3.879(+11)	2.714(+4)	3.745(−1)	1.123(−13)	0.3047
9.885(−4).....	3.676	2.806	7.312	2.119	0.3056
2.595(−3).....	3.494	2.891	1.386(+0)	3.897	0.3066
5.308.....	3.328	2.927	2.570	7.149	0.3077
9.813.....	3.178	2.970	4.684	1.286(−12)	0.3096
2.882(−2).....	2.914	3.054	1.408(+1)	3.762	0.3176
4.668.....	2.798	3.097	2.268	5.991	0.3241
7.267.....	2.691	3.143	3.435	8.949	0.3318
1.082(−1).....	2.592	3.191	4.863	1.247(−11)	0.3398
3.381.....	2.258	3.433	1.135(+2)	2.696	0.3602
6.490.....	2.002	3.733	1.868	4.064	0.3629
1.011(+0).....	1.797	4.055	2.923	5.846	0.3621
2.066.....	1.461	4.881	7.835	1.301(−10)	0.3585
3.046.....	1.299	5.551	1.499(+3)	2.189	0.3562
4.097.....	1.189	6.195	2.502	3.273	0.3556
5.970.....	1.063	7.195	4.614	5.197	0.3579
7.890.....	9.749(+10)	8.067	6.896	6.930	0.3607
1.000(+1)	9.000	8.866	9.576	8.755	0.3618

NOTE.—Numbers in parentheses indicate powers of 10.

TABLE 5

GRAY MODEL 2: $T(2/3) = 53558$

τ_R	R (cm)	T (° K)	P (dyn cm^{-2})	ρ (g cm^{-3})	$\langle\kappa_R\rangle$ (cm^2 g^{-1})
.....	1.939(+11)	3.117(+4)	8.406(−1)	2.187(−13)	0.3068
1.043(−3).....	1.838	3.215	1.838(+0)	4.636	0.3075
2.910.....	1.746	3.315	3.866	9.457	0.3087
6.351.....	1.664	3.417	7.765	1.843(−12)	0.3106
1.231(−2).....	1.589	3.523	1.476(+1)	3.397	0.3133
5.902.....	1.399	3.882	6.760	1.412(−11)	0.3244
1.261(−1).....	1.296	4.159	1.358(+2)	2.647	0.3304
2.263.....	1.207	4.460	2.325	4.226	0.3337
4.392.....	1.094	4.943	4.455	7.306	0.3357
7.289.....	1.001	5.459	7.711	1.145(−10)	0.3366
1.098(+0).....	9.221(+10)	5.999	1.234(+3)	1.667	0.3378
2.048.....	7.967	7.099	2.496	2.849	0.3418
2.964.....	7.156	7.966	3.694	3.759	0.3438
3.923.....	6.495	8.771	5.134	4.746	0.3434
4.931.....	5.946	9.546	7.170	6.089	0.3418
6.032.....	5.482	1.033(+5)	1.018(+4)	7.991	0.3402
8.104.....	4.874	1.166	1.826	1.270(−9)	0.3377
1.002(+1).....	4.500	1.281	2.865	1.812	0.3352

NOTE.—Numbers in parentheses indicate powers of 10.

TABLE 6

NONGRAY MODEL 2: $T(2/3) = 48865$

τ_R	R (cm)	T (° K)	P (dyn cm^{-2})	ρ (g cm^{-3})	$\langle\kappa_R\rangle$ (cm^2 g^{-1})
.....	1.939(+11)	3.543(+4)	9.976(−1)	2.282(−13)	0.3066
1.062(−3).....	1.838	3.590	2.064(+0)	4.661	0.3070
2.908.....	1.746	3.662	4.185	9.262	0.3078
6.246.....	1.664	3.734	8.251	1.791(−12)	0.3090
1.204(−2).....	1.588	3.804	1.570(+1)	3.347	0.3111
6.120.....	1.399	4.012	7.779	1.572(−11)	0.3236
9.463.....	1.345	4.071	1.147(+2)	2.284	0.3294
2.539(−1).....	1.207	4.305	2.455	4.624	0.3411
4.756.....	1.094	4.614	3.955	6.950	0.3438
7.407.....	1.001	4.993	6.028	9.786	0.3431
1.052(+0).....	9.221(+10)	5.450	9.185	1.366(−10)	0.3418
2.009.....	7.791	6.840	2.277(+3)	2.698	0.3419
3.043.....	6.876	8.141	3.978	3.961	0.3439
4.003.....	6.264	9.012	5.831	5.244	0.3436
5.065.....	5.751	9.815	8.447	6.977	0.3425
6.012.....	5.398	1.046(+5)	1.138(+4)	8.821	0.3415
7.952.....	4.874	1.165	1.931	1.344(−9)	0.3395
1.000(+1).....	4.500	1.274	3.055	1.943	0.3379

NOTE.—Numbers in parentheses indicate powers of 10.

TABLE 7

GRAY MODEL 3: $T(2/3) = 82180$

τ_R	R (cm)	T (° K)	P (dyn cm^{-2})	ρ (g cm^{-3})	$\langle\kappa_R\rangle$ (cm^2 g^{-1})
.....	1.078(+11)	4.828(+4)	2.496(+0)	4.191(−13)	0.3069
1.652(−3).....	1.004	5.032	7.285	1.174(−12)	0.3075
3.198.....	9.704(+10)	5.135	1.209(+1)	1.909	0.3079
8.971.....	9.101	5.349	3.115	4.772	0.3093
1.394(−2).....	8.827	5.462	4.811	7.143	0.3102
3.049.....	8.325	5.702	1.049(+2)	1.492(−11)	0.3125
5.945.....	7.878	5.967	2.007	2.728	0.3152
1.041(−1).....	7.476	6.256	3.363	4.358	0.3181
3.728.....	6.343	7.346	9.612	1.061(−10)	0.3242
6.819.....	5.614	8.258	1.615(+3)	1.586	0.3248
1.040(+0).....	5.035	9.158	2.601	2.303	0.3243
1.980.....	4.174	1.108(+5)	6.766	4.952	0.3229
2.992.....	3.699	1.272	1.381(+4)	8.807	0.3217
4.058.....	3.399	1.415	2.406	1.378(−9)	0.3207
5.953.....	3.078	1.625	4.892	2.441	0.3194
8.001.....	2.867	1.809	8.413	3.771	0.3184
1.029(+1).....	2.708	1.982	1.323(+5)	5.412	0.3175
1.267.....	2.588	2.138	1.908	7.237	0.3170
1.495.....	2.500	2.277	2.536	9.034	0.3164

NOTE.—Numbers in parentheses indicate powers of 10.

TABLE 8

NONGRAY MODEL 3: $T(2/3) = 95090$

τ_R	R (cm)	T (° K)	P (dyn cm^{-2})	ρ (g cm^{-3})	$\langle\kappa_R\rangle$ (cm^2 g^{-1})
.....	1.078(+11)	7.123(+4)	3.472(+0)	3.952(−13)	0.3062
1.290(−3).....	1.004	7.236	7.157	8.018	0.3063
3.555.....	9.393(+10)	7.352	1.451(+1)	1.600(−12)	0.3065
7.494.....	8.827	7.471	2.884	3.130	0.3068
1.042(−2).....	8.569	7.533	4.031	4.337	0.3072
2.555.....	7.877	7.728	1.048(+2)	1.099(−11)	0.3084
7.242.....	7.112	8.025	3.193	3.224	0.3115
1.143(−1).....	6.783	8.198	5.095	5.037	0.3135
3.934.....	5.837	8.964	1.630(+3)	1.473(−10)	0.3195
7.131.....	5.308	9.604	2.775	2.342	0.3214
1.027(+0).....	4.949	1.014(+5)	3.922	3.134	0.3220
2.017.....	4.234	1.159	8.299	5.804	0.3220
3.048.....	3.795	1.287	1.454(+4)	9.163	0.3214
4.002.....	3.522	1.391	2.201	1.283(−9)	0.3208
6.058.....	3.144	1.586	4.372	2.235	0.3197
7.960.....	2.924	1.742	7.052	3.282	0.3188
9.994.....	2.758	1.891	1.059(+5)	4.589	0.3180
1.249(+1).....	2.611	2.060	1.585	6.237	0.3171
1.500.....	2.500	2.217	2.210	8.080	0.3163

NOTE.—Numbers in parentheses indicate powers of 10.

a) Temperature Stratifications

Figure 1 shows a typical temperature stratification for the spherical models. Plotted is $B(= \sigma^* T^4/\pi)$ versus mean optical depth. Also shown are the plane-parallel distributions

$$B = \tfrac{3}{4} \frac{L}{4\pi^2 R_{\min}{}^2} (\tau + \tfrac{2}{3}) , \tag{51}$$

$$B = \tfrac{3}{4} \frac{L}{4\pi^2 R_{\max}{}^2} (\tau + \tfrac{2}{3}) . \tag{52}$$

Note that the spherical temperature stratifications are almost completely enveloped by the two plane-parallel stratifications. There is a much larger range in temperature down to optical depth unity in a spherical atmosphere than in a plane-parallel one, as one might expect. For example, for gray model 2, the temperature goes from 3.2×10^4 ° to 6×10^4 ° K in this optical depth range. Setting $T_{\rm eff} = T(\tau = \frac{2}{3})$ and using equation (2), we find the corresponding temperatures for the gray planar atmosphere to be 4.25×10^4 ° to 5.2×10^4 ° K. This wide range of temperatures in extended atmospheres may be important in explaining the appearance of ions with very different ionization potentials that are seen in the spectra of some central stars (Smith and Aller 1969).

For all three models, the temperature at small optical depths is larger for the nongray models than for the gray models. This is contrary to the usual case in plane-parallel calculations. However, Unno (1963) notes that even in plane-parallel calculations the nongray surface temperature may in some cases be larger than the gray surface temperature if the absorption k_ν is distributed with frequency such that the atmosphere is more transparent on the red side than on the violet side of the maximum of the Planck function.

For the spherical models calculated here, the increase in the surface temperature in the nongray case is due in part to the very steep gray temperature gradient $dB/d\tau$ near the surface (Fig. 1), and in part to the large contribution of electron scattering to the

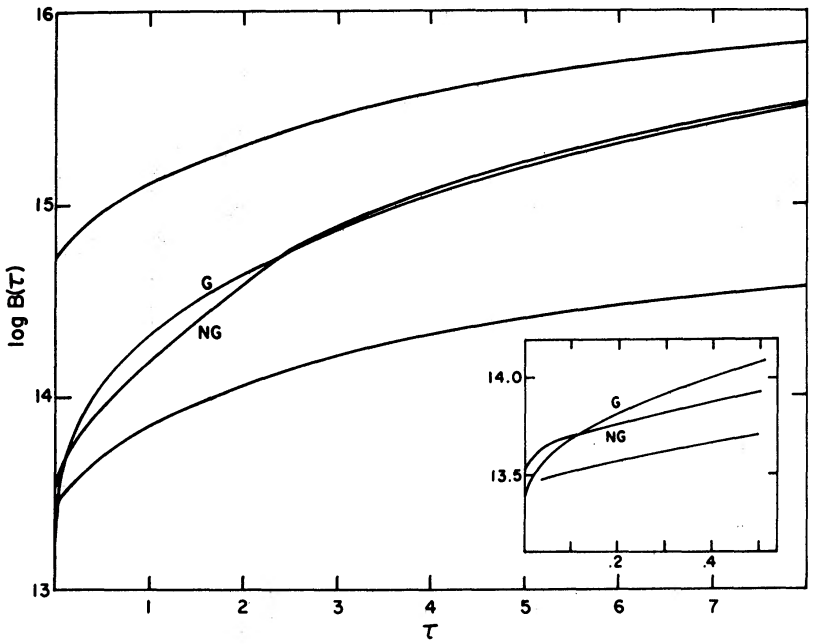

FIG. 1.—$B(\tau)$ stratification for gray model 2 and nongray model 2. The two curves which envelop the spherical solutions are plane-parallel stratifications, equations (51) and (52). *Insert*, region near the surface with the scale of the ordinate expanded by a factor of 5.

opacity. As is well known (Kourganoff 1952), the mean intensity tends to be larger than B_ν toward violet frequencies because of the rapid increase of B_ν with depth. This excess of J_ν over B_ν is exaggerated if coherent scattering is an important source of opacity, for then the radiation field J_ν near the surface has a large contribution from photons which have traveled, in random-walk fashion, from large depths, where B_ν is weighted heavily toward short wavelengths.

The net effect of the steep gray temperature gradient and the coherent scattering by electrons is that in the initial nongray calculation J_ν tends to be much larger than B_ν at short wavelengths. This in turn affects the nongray temperature stratification, as may be seen by considering the radiative-equilibrium condition

$$\int_0^\infty \kappa_\nu J_\nu d\nu = \int_0^\infty \kappa_\nu B_\nu d\nu \,. \tag{53}$$

For this to be satisfied, B_ν increases and the nongray surface temperature is made larger than the gray surface temperature.

b) The Emergent-Flux Distributions

Figures 2–4 show the emergent-flux distributions for the nongray stratifications. The

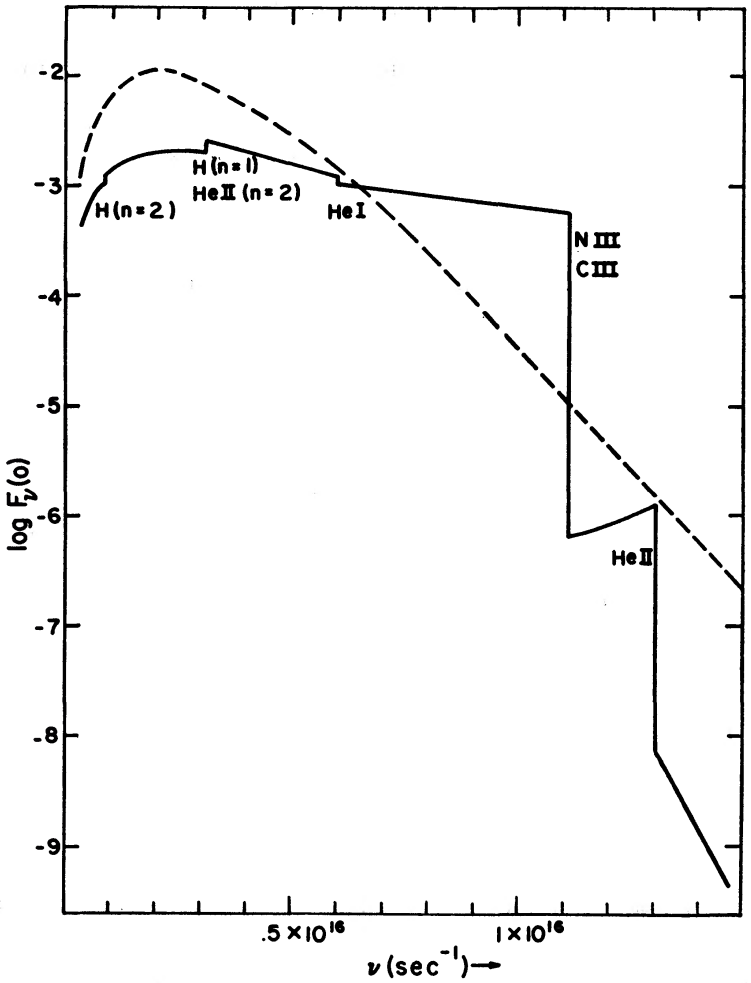

FIG. 2.—Emergent flux versus frequency for nongray model 1. *Dashed line*, blackbody distribution for the temperature at $\tau = \frac{2}{3}$; $T(\frac{2}{3}) = 37496$.

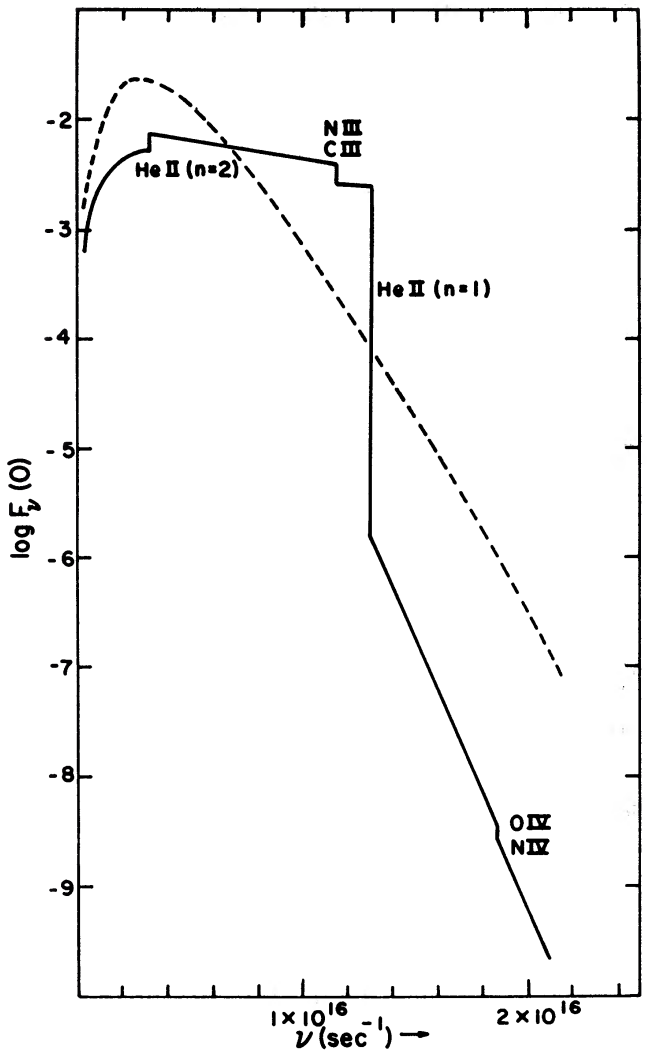

FIG. 3.—Emergent flux versus frequency for nongray model 2. Shown for comparison is the blackbody distribution for $T(\frac{2}{3}) = 48865$

flux distributions show strong absorption edges in the far-ultraviolet and emission edges in the visual and near-ultraviolet. These features may be understood on the basis of geometrical effects and the Schuster mechanism.

The abrupt increase in κ_ν as we pass through an ionization edge in going from longer to shorter wavelengths usually leads to an absorption edge, a decrease in $F_\nu(0)$; one looks deeper into the atmosphere on the long-wavelength side of the edge than on the shortward side and thus sees down to a depth where B_ν is larger. For a spherical model this is counterbalanced to some extent by the fact that the observed flux is proportional to πR^2, where R is the radius of the observed disk, say at $(\tau_\nu)_{\text{tangential}} = 1$. The observed disk is larger for larger κ_ν. Gebbie and Thomas (1968) refer to this phenomenon as "geometrically induced emission." The very large absorption edges in the ultraviolet regions of our models show that the rapid decrease in B_ν more than makes up for this geometrical effect. The increase in the area of the observed disk increases as R^2, but the decrease in $B_\nu(R)$ in the ultraviolet is more rapid than $1/R^2$.

At wavelengths considerably longer than the wavelength corresponding to the maximum of the Planck function, B_ν does not decrease as rapidly with radius, so geometrically

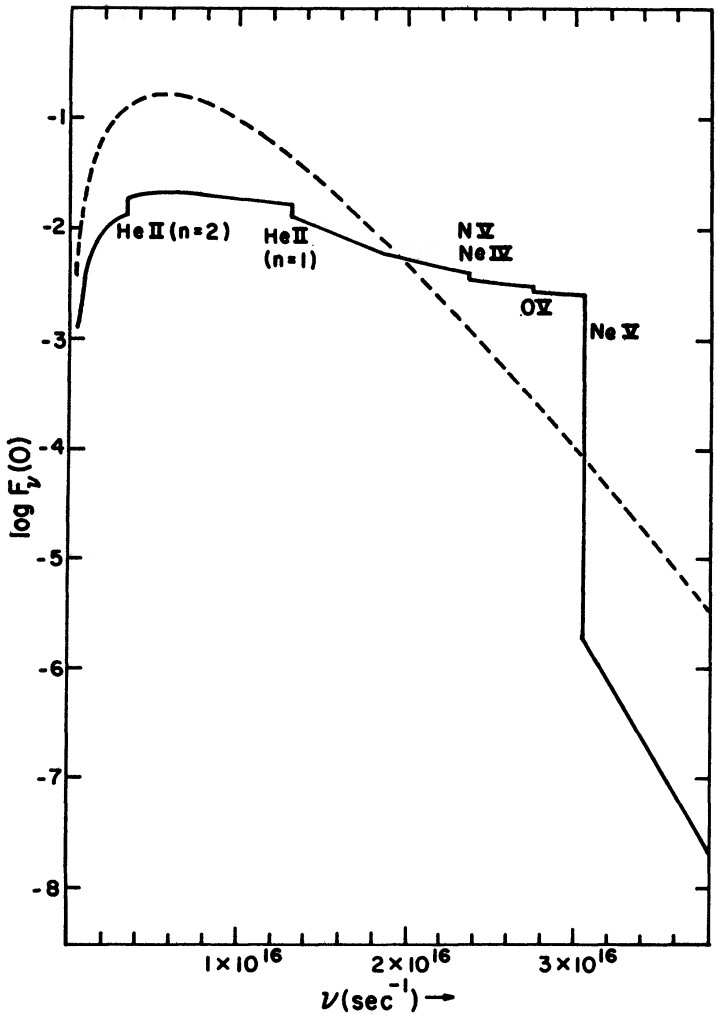

FIG. 4.—Emergent flux versus frequency for nongray model 3. Shown for comparison is the blackbody distribution for $T(\frac{2}{3}) = 95090$.

induced emission may be important there. It is also important to note that this is the same frequency region at which the Schuster mechanism is important, so the emission edges found here might be described as being due to a geometrically enhanced Schuster mechanism. The Schuster mechanism has been discussed by Gebbie (1967), who found an emission edge at the Lyman limit in her plane-parallel models of central stars; by Gebbie and Thomas (1968); and by Böhm (1968). The operation of this mechanism depends on the fact that in an atmosphere in which scattering is important the source function is given by equation (20). The source function S_ν may increase across an absorption edge, jumping from a value near J_ν to a larger value near B_ν. (It is toward the red region of the spectrum that J_ν is smaller than B_ν.) If this jump in S_ν occurs in a large part of the atmosphere, an emission edge may show up in the emergent flux $F_\nu(0)$.

All three models show emission edges at the Balmer and Lyman limits. For models 1, 2, and 3 the emission of the Balmer edge is 0.13, 0.08, and 0.03 mag, respectively. Liller (1970) informs us that he observed the Balmer edge in emission by about a tenth of a magnitude in a central star and in a B3 Ia supergiant, but this was while he was using Vega as a standard and using the old calibration of Oke (1964). The more recent calibra-

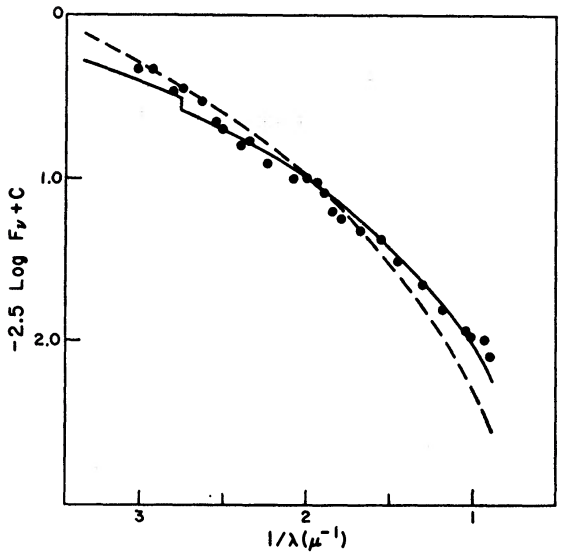

FIG. 5.—Comparison of the energy distribution of nongray model 2 (*solid line*) with the continuous energy distribution of the Wolf-Rayet star HD 191765 (WN6) (*solid dots*). The discontinuity is the Balmer edge which appears in emission for the spherical models calculated here. *Dashed line*, blackbody distribution for $T = 48865°$ K.

tions of Vega by Hayes (1970) and Oke and Schild (1970) have decreased the absolute energy distribution just shortward of λ3647 by 0.09 mag, enough to null the emission edge detected by Liller.

The strong absorption edges in the far-ultraviolet agree at least qualitatively with the results of plane-parallel models. It is interesting to note, however, that nongray model 3 (Fig. 4) shows an excess of ultraviolet radiation just beyond the Ne IV edge. Williams (1968) notes that just such an excess is required to explain the Ne V emission lines which are observed in those planetary nebulae which have central stars with $T_{\rm eff} \approx 9 \times 10^4$ ° K.

The energy-flux distributions from the spherical models are rather "flat," compared with the plane-parallel results (cited in the Introduction) which more closely mimic the blackbody distribution. Kuhi (1966) found that the emergent continuum of Wolf-Rayet stars also deviates rather strongly from a blackbody distribution. Since Wolf-Rayet stars are generally thought to have extended atmospheres, it is perhaps of some interest to compare the calculated $F_\nu(0)$ with Kuhi's observations, though we should note that the models calculated in this paper were not intended to be for Wolf-Rayet stars. Figure 5 shows the emergent flux in the visual and infrared as calculated from the stratification of model 2, along with observational data on HD 191765 (WN5). The distributions match reasonably well. The model has the excess radiation in the infrared required to fit the Wolf-Rayet continuum. This radiation originates in the cool outer layers of the atmosphere. Note also the emission at the Balmer edge. This edge does not appear in Kuhi's observations, but such an edge would perhaps be smoothed out by the strong expansion motions known to exist in Wolf-Rayet atmospheres.

I would like to express my deepest gratitude to Dr. Karl-Heinz Böhm for introducing me to this problem and for his constant advice and encouragement throughout the course of the investigation. I am grateful to Dr. J. A. Stoddard for the loan of his discrete ordinate sub-routine. Many fruitful discussions were held with Drs. E. Böhm-Vitense, N. J. McCormick, J. Schmid-Burgk, and G. Wallerstein.

This study has been supported by NSF grants GP 8145 and GP 11606. The computer time was provided by the College of Arts and Sciences of the University of Washington.

APPENDIX

THE DISCRETE-S_N EQUATIONS

In the notation of radiative transfer the discrete-S_N representation of the transfer equation is

$$\mu_m \frac{A_{i+1}I_{i+1} - A_iI_i}{V_i} + \frac{\alpha_{m+1/2}I_{m+1/2} - \alpha_{m-1/2}I_{m-1/2}}{V_iw_m} + k\rho I = k\rho S ,$$

where for the net of points (r_i, μ_m) and for any function $f(r_i, \mu_m)$ we let

$$f_i = f(r_i, \mu_m) , \quad f_{m+1/2} = f(r_{i+1/2}, \mu_{m+1/2}) ,$$

and where

$$V_i = \frac{4\pi}{3}(r_{i+1}^3 - r_i^3) , \quad A_i = 4\pi r_i^2 , \quad R_{\min} = r_1 < r_2 < \ldots < r_{L+1} = R_{\max} .$$

The $\mu_m (m = 1, \ldots, M)$ are direction cosines. The curvature coefficients α are defined recursively as

$$\frac{\alpha_{m+1/2} - \alpha_{m-1/2}}{w_m} = -\mu_m(A_{i+1} - A_i) , \quad \alpha_{1/2} = \alpha_{M+1/2} = 0 .$$

REFERENCES

Böhm, K. H. 1968, in *I.A.U. Symposium No. 34: Planetary Nebulae*, ed. D. E. Osterbrock and C. R. O'Dell (Dordrecht: Reidel Publishing Co.), p. 297.
———. 1969, *Astr. and Ap.*, **1**, 180.
Böhm, K. H., and Cassinelli, J. P. 1970, in *Spectrum Formation in Stars with Steady State Extended Atmospheres*, ed. H. G. Groth and P. Wellman (Washington: U.S. Government Printing Office), p. 54
Böhm, K. H., and Deinzer, W. 1965, *Zs. f. Ap.*, **61**, 1.
———. 1966, *ibid.*, **63**, 177.
Carlson, B. G. 1963, *Methods of Computational Physics*, Vol. 1 (New York: Academic Press), p. 1.
Carlson, B. G., and Lathrop, K. D. 1968, in *Computing Methods in Reactor Physics*, ed. H. Greenspan, C. N. Kelber, and D. Okrent (New York: Gordon & Breach), p. 171.
Chamberlain, J. W. 1963, *Planetary and Space Sci.*, **10**, 901.
Chandrasekhar, S. 1950, *Radiative Transfer* (London: Oxford University Press).
Chapman, R. D. 1964, Air Force Cambridge Research Laboratories, Office of Aerospace Research, Report No. AFCRL-64-961.
———. 1966, *Ap. J.*, **143**, 61.
Gebbie, K. B. 1967, *M.N.R.A.S.*, **135**, 181.
Gebbie, K. B., and Seaton, M. J. 1963, *Nature*, **199**, 580.
Gebbie, K. B., and Thomas, R. N. 1968, *Ap. J.*, **154**, 285.
Gelbard, E. M., and Hageman, L. A. 1969, *Nucl. Sci. Eng.*, **37**, 288.
Hamming, R. W. 1962, *Numerical Methods for Scientists and Engineers* (New York: McGraw-Hill Book Co.).
Hayes, D. S. 1970, *Ap. J.*, **159**, 165.
Hummer, D. G., and Mihalas, D., 1970, *M.N.R.A.S.*, **147**, 339.
Kosirev, N. A., 1934, *M.N.R.A.S.*, **94**, 430.
Kourganoff, V. 1952, *Basic Methods in Transfer Problems* (London: Oxford University Press).
Krook, M. 1955, *Ap. J.*, **122**, 488.
Kuhi, L. V. 1966, *Ap. J.*, **143**, 753.
Lathrop, K. D. 1965, Los Alamos Sci. Lab. Rept., LA-3373.
Liller, W. 1970, private communication.
Lucy, L. B. 1964, *Smithsonian Ap. Obs. Spec. Rept.*, No. 167, p. 93.
Mihalas, D. 1967, *Methods in Computational Physics*, Vol. 7 (New York: Academic Press), p. 1.
Oke, J. B. 1964, *Ap. J.*, **140**, 689.
Oke, J. B., and Schild, R. E. 1970, *Ap. J.*, **161**, 1015.
Schmid-Burgk, J. 1970, private communication.
Smith, L. F., and Aller, L. H. 1969, *Ap. J.*, **157**, 1245.
Stoddard, J. A. 1969, unpublished Ph.D. Thesis, University of Washington.
Unno, W. 1963, *Pub. Astr. Soc. Japan*, **15**, 400.
Unsöld, A. 1951, *Naturwiss.*, **22**, 525.
Wachspress, E. L. 1966, *Iterative Solution of Elliptic Systems* (Englewood Cliffs, N.J.: Prentice-Hall, Inc.), p. 70.
Wentzel, D. G. 1970, *Ap. J.*, **160**, 373.
Williams, R. E. 1968, in *I.A.U. Symposium No. 34: Planetary Nebulae*, ed. D. E. Osterbrock and C. R. O'Dell (Dordrecht: Reidel Publishing Co.), p. 190.